Modeling of the Centerless Through-feed Grinding Process

Kang Kim*

School of Mechanical and Automotive Engineering, Kookmin University,
861-1 Jungreung-dong, Sungbook-gu, Seoul 136-702, Korea

A computer simulation method for investigating the form generation mechanism in the centerless through-feed grinding process is described. The length of the contact line and the magnitude of the grinding force between the grinding wheel and workpieces, vary with the change in the axial location of the current workpiece during grinding. Thus, a new coordinate system and a grinding force curve of previous and/or following workpieces are introduced to treat the axial motion. Experiments and computer simulations were carried out using four types of cylindrical workpiece shapes. To validate this model, simulation results are compared with the experimental results.

Key Words : Centerless Through-feed Grinding, Axial Motion of Workpiece, Cylindricity

1. Introduction

Centerless through-feed grinding is accomplished by passing the workpiece between the grinding and regulating wheels. Grinding takes place as the workpiece passes from one side of the wheels to the other. The representative theoretical researches about rounding mechanisms in centerless grinding were presented by Dall (1946), Yonetsu (1959), and by Rowe and Barash (1964). Their researches were based on the infeed grinding process, and were limited to 2-D modeling to investigate the influences of centerless grinding variables on the out-of-roundness of the ground part. Theoretical researches on the through-feed process were also done by Yonetsu (1960) and Meis (1980) based on 2-D analysis.

The objective of this research is to develop a 3-D computer simulation method for a cylindrical form generation mechanism in a centerless through-feed grinding process. The basic concepts

* E-mail : kangkim@kookmin.ac.kr
  TEL : +82-2-910-4676; **FAX :** +82-2-910-4839
  School of Mechanical and Automotive Engineering, Kookmin University, 861-1 Jungreung-dong, Sungbook-gu, Seoul 136-702, Korea (Manuscript **Received** February 3, 2003; **Revised** April 14, 2003)
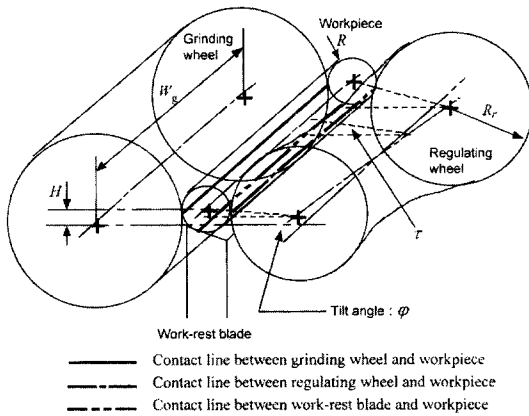
of the apparent depth of cut, the interference restrictions, the machining elasticity, and the contact line modeling presented in Kim, Chu, and Barash's researches (1992a, 1992b) are adopted in this work. The 3-D through-feed model is complicated because the length of the contact line and the magnitude of the grinding force between the grinding wheel and the workpieces vary with the change of the axial location of the workpiece during grinding. Hence, a new coordinate system, variable stages of grinding procedure, and a grinding force curve of previous and/or following workpieces are introduced to treat the axial motion of the workpiece during this process. The basic assumptions behind this model are :

(1) The effect of vibration is ignored ;

(2) Wear of wheels and work-rest blade is ignored ;

(3) Angular velocity of workpiece is constant ; and

(4) Linear velocity of workpiece during through-feed grinding is constant.

2. Instantaneous Change of Apparent Depth of Cut

The through-feed grinding is performed by passing the workpiece through the gap between

Fig. 1   Schematic diagram of through-feed grinding

Fig. 2   Coordinate system for through-feed grinding

the grinding wheel and the regulating wheel as shown in Fig. 1. To generate axial motion of the workpiece the regulating wheel is tilted with respect to the workpiece axis and has a hyperboloid ruled surface (Yonetsu, 1960). Generally, the regulating wheel tilt angle, φ, is only a few degrees and the size of the wheel is much larger than that of the workpiece. The difference between its maximum and minimum diameter is very small and the diameter can be regarded as a constant. The change of the angle, π, between the regulating wheel contact normal and the horizontal line is somewhat larger, but the workpiece center height angle, β, is kept the same in the workpiece. Therefore, the variation of τ has no effect on the form generation mechanism.

Figure 2 shows the coordinate system of the through-feed grinding process. Also, Fig. 3 shows the simplified 2-D configuration of the centerless grinding geometry where θ is the angle of rotation ($\angle O_gOX$) between the initial reference line OX on the work-piece and the grinding wheel contact normal shown as OO_g. In Fig. 3, α is the angle ($\angle O_gOB$) between the line OO_g and the normal line OB of the work-rest blade surface, β is the supplementary angle ($\pi - \angle O_gOO_r$) between the line OO_r connecting the work-piece center and the regulating wheel center and the line OO_g, and γ is the top angle of the work-rest blade. The reference line OX coincides with the line OO_g at the beginning of grinding.
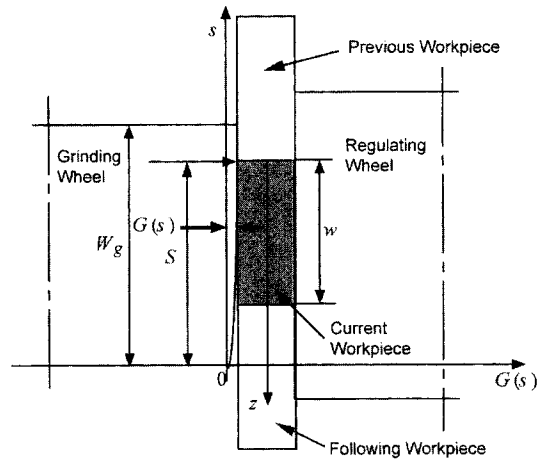
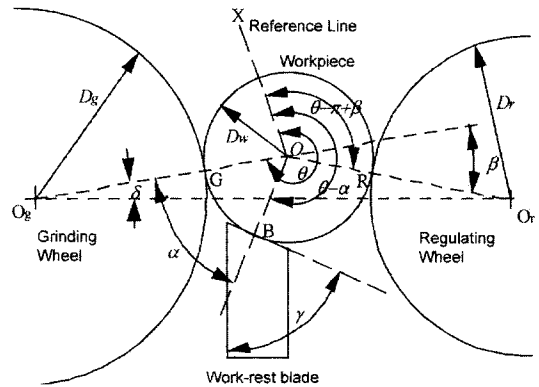In this work, $r(\theta, z_i)$ is defined as the distance

Fig. 3   Centerless grinding geometry

from any reference point, O, in the cross-section of the workpiece at an axial distance z_i from the leading end to the periphery of the workpiece at angle θ from the reference line OX. When the irregularities of the workpiece arrive either at the work-rest blade or at the regulating wheel, the workpiece is displaced, and the apparent depth of cut at the grinding wheel contact point will be changed. Also, the apparent depth of cut is changed by the grinding wheel shape function $G(s)$.

The surface of a cylindrical part shows not only circumferential waviness but also axial waviness. Thus, for 3-D modeling, it is required to consider all contact points at the grinding wheel, regulating wheel, and work-rest blade. An averaging concept defining a least squares contact line

(LSCL) is used in this work (Kim et al., 1992b).

Also, there are interference phenomena in a centerless grinding process (Kim et al., 1992b). Thus, if the angular displacement difference between the real regulating wheel contact point at rotation θ and its ideal contact point, $r(\theta-\pi+\beta, z_i)$, is ξ_{θ,z_i}, the LSCL equation for the regulating wheel contact line, $C_0^w(\theta-\pi+\beta, z)$, is:

$$C_0^w(\theta-\pi+\beta, z) = A_r + B_r z \quad (0 \leq z \leq w) \quad (1)$$

$$A_r = [\sum\{\cos(\xi_{\theta,z_i}) r(\theta-\pi+\beta+\xi_{\theta,z_i}, z_i)\}]/n - B_r\{\sum z_i\}/n \quad (2)$$

$$B_r = \frac{\sum\{z_i\{\cos(\xi_{\theta,z_i}) r(\theta-\pi+\beta+\xi_{\theta,z_i}, z_i)\}\} - [\{\sum z_i\}\{\sum(\cos(\xi_{\theta,z_i}) r(\theta-\pi+\beta+\xi_{\theta,z_i}, z_i)\}\}/n]}{\sum z_i^2 - \{\sum z_i\}^2/n}$$

$$\left(0 \leq z_i \leq w, \ n = \frac{w}{\Delta z}\right)$$
(3)

where n is the number of measurement layers and w is the length of the workpiece,

Similarly, if the angular displacement difference between the real work-rest blade contact point and its ideal contact point, $r(\theta-\alpha, z_i)$, is ζ_{θ,z_i}, LSCL equation for the work-rest blade contact line, $C_0^w(\theta-\alpha, z)$, can be expressed as

$$C_0^w(\theta-\alpha, z) = A_b + B_b z \quad (0 \leq z \leq w) \quad (4)$$

$$A_b = [\sum\{\cos(\zeta_{\theta,z_i}) r(\theta-\alpha+\zeta_{\theta,z_i}, z_i)\}]/n - B_b\{\sum z_i\}/n \quad (5)$$

$$B_b = \frac{\sum\{z_i\{\cos(\zeta_{\theta,z_i}) r(\theta-\alpha+\zeta_{\theta,z_i}, z_i)\}\} - [\{\sum z_i\}\{\sum(\cos(\zeta_{\theta,z_i}) r(\theta-\alpha+\zeta_{\theta,z_i}, z_i)\}\}/n]}{\sum z_i^2 - \{\sum z_i\}^2/n}$$

$$\left(0 \leq z_i \leq w, \ n = \frac{w}{\Delta z}\right)$$
(6)

If there are no previous and/or following workpieces, the instantaneous changes of apparent depth of cut at the grinding wheel contact points can be expressed as a sum of the change of the grinding wheel shape and the effects of the irregularities at the work-rest blade contact point, regulating wheel contact point, and grinding wheel contact point (Kim et al., 1992b). Then, the instantaneous change in the apparent depth of cut, $D(\theta, \eta, z)$, in $\Delta\theta$ rotation can be expressed as:

$$D(\theta, \eta, z) = T[D(\theta-\Delta\theta, 0, z) + \{G(S-z) - G(S-z-R\Delta\theta\sin\varphi)\}$$
$$-\frac{\sin\beta}{\sin(\alpha+\beta)}\{C_0^w(\theta-\alpha, z) - C_0^w(\theta-\alpha-\Delta\theta, z)\}$$
$$+\frac{\sin\alpha}{\sin(\alpha+\beta)}\{C_0^w(\theta-\pi+\beta, z) - C_0^w(\theta-\pi+\beta-\Delta\theta, z)\}$$
$$+\{\cos(\eta) r(\theta+\eta, z) - r(\theta+\eta-\Delta\theta, z)\}]$$
(7)

where R is the radius of the workpiece and η is the angular displacement difference between the real grinding wheel contact point and the ideal contact point.

The followings are the conditions for each stage:

At the first stage $(S < w)$ $T=1$ (when $z \leq S$)
                                 $T=0$ (when $z > S$)
At the second stage $(w \leq S \leq W_g)$ $T=1$
At the third stage $(S > W_g)$ $T=0$ (when $z < S - W_g$)
                                 $T=1$ (when $z \geq S - W_g$)

where S is the axial distance from the initial workpiece contact point of the grinding wheel to the leading end of the workpiece and T is a dummy parameter which is used to separate the equation for the non-contact surface.

3. Grinding Force of Previous and/or Following Workpieces and Global Deflection

The through-feed grinding process is composed of three stages. The first stage starts just after the leading end of the workpiece contacts the wheels and finishes when the full length of the workpiece is in contact with both wheels. The second stage starts right after the first stage and finishes when the leading end of workpiece leaves the grinding wheel. The third stage also starts just after the second stage and finishes when the trailing end of the workpiece leaves the grinding wheel.

During through-feed grinding, the workpieces are fed to a centerless grinding machine continuously. After a certain time from the start, the space between the wheels is filled with a series of workpieces. If the variation in the workpiece external shape is small, the normal grinding force distribution along the grinding wheel axis can be assumed as a continuous curve given by $f_{ss}(s)$.

Using the equivalent 2-D infeed model (Kim et al., 1992a) and machining elasticity parameter, $f_{ss}(s)$ can be found. From the grinding wheel shape function, $G(s)$, and the regulating wheel tilt angle, φ, the equivalent infeed grinding condition (infeed rate and number of workpiece rotations) is derived. The equivalent workpiece length of the infeed grinding process is equal to the axial displacement of the current workpiece during one revolution of this current workpiece. The force, $F_c(S)$, which is applied to the machine system by the previous and/or following workpieces when the leading end of the current workpiece reaches S, is gvien as :

$$F_c(S) = \int_0^a f_{ss}(s)\,ds + \int_b^{W_g} f_{ss}(s)\,ds$$
$$\begin{pmatrix} if\ S-w>0 & a=S-w, & if\ S-w\le0 & a=0 \\ if\ S<W_g & b=S, & if\ S\ge W_g & b=0 \end{pmatrix} \quad (8)$$

where W_g is the width of the grinding wheel and a and b are dummy parameters that define the range of the integration.

The force, $F_c(S)$, causes an elastic deflection of the machine system. It is assumed that this global deflection is parallel to the axis of the grinding wheel. The amount of this global deflection, $D_c(S)$, when the leading end of this workpiece reaches S, is expressed as :

$$D_c(S) = \frac{F_c(S)}{K_e} \quad (9)$$

where K_e is the elasticity factor of the system.

The deflection of the machine system due to the current workpiece is the difference between the maximum apparent depth of cut, $D(\theta, \eta_{max}, z_i)$, and the maximum true depth of cut, $L(\theta, \eta_{max}, z_i)$. The grinding force of each layer is approximated by multiplying the deflection by the elasticity factor. The total grinding force, $F_n(S)$ is also expressed as the sum of $F_c(S)$ and $F_o(S)$, which is the normal grinding force which causes material removal of the current workpiece. If the number of layers of the current workpiece being ground is l_e, $F_o(S)$ can be expressed as :

$$F_o(S) = F_n(S) - F_c(S)$$
$$\cong \frac{K_e}{l_e}\left[\sum_{for\ all\ G.W.\ contact\ layers}\{D(\theta, \eta_{max}, z_i) - L(\theta, \eta_{max}, z_i)\}\right] - F_c(S)$$

$$=\frac{K_e}{l_e}\left[\sum_{for\ all\ G.W.\ contact\ layers}\left\{D(\theta, \eta_{max}, z_i) - \frac{F_c(S)}{K_e}\right\} - L(\theta, \eta_{max}, z_i)\right]$$
$$=\frac{K_e}{l_e}\left[\sum_{for\ all\ G.W.\ contact\ layers}\{D(\theta, \eta_{max}, z_i) - D_c(S)\} - L(\theta, \eta_{max}, z_i)\right]$$
$$=\frac{K_e}{l_e}\left[\sum_{for\ all\ G.W.\ contact\ layers}\{D_e(\theta, \eta_{max}, z_i) - L(\theta, \eta_{max}, z_i)\}\right] \quad (10)$$

As a result, the apparent depth of cut of the current workpiece is reduced by $D_c(S)$, because of $F_c(S)$. Therefore, the effective apparent depth of cut, $D_e(\theta, \eta, z_i)$, is

$$D_e(\theta, \eta, z_i) = D(\theta, \eta, z_i) - D_c(S) \quad (11)$$

4. 3-D Through-feed Model

During a continuous through-feed process, the normal grinding force which is applied to the current workpiece, $F_o(S)$, is always less than the total grinding force, $F_n(S)$, because of the previous and/or following workpieces. The effective apparent depth of cut, $D_e(\theta, \eta, z)$, is calculated using Eq. (11). Then, the effective deflection force, which is equal to $F_o(S)$, can be found by using $D_e(\theta, \eta_{max}, z)$.

Therefore, by modifying the 3-D infeed model (Kim et al. 1992b), $D_e(\theta, \eta, z)$ can be given as

$$D_e(\theta, \eta, z) = T^r D(\theta - \Delta\theta, 0, z) + \{G(S-z) - G(S-z-R\Delta\theta\sin\varphi)\} - D_c(S)$$
$$\quad -\frac{\sin\beta}{\sin(\alpha+\beta)}\{C_o^w(\theta-\alpha, z) - C_o^w(\theta-\alpha-\Delta\theta, z)\}$$
$$\quad +\frac{\sin\alpha}{\sin(\alpha+\beta)}\{C_o^w(\theta-\pi+\beta, z) - C_o^w(\theta-\pi+\beta-\Delta\theta, z)\} \quad (12)$$
$$\quad +\{\cos(\eta)r(\theta+\eta, z) - r(\theta+\eta-\Delta\theta, z)\}]$$

where $\{G(S-z) - G(S-z-R\Delta\theta\sin\varphi)\}$ corresponds to the amount of infeed during $\Delta\theta$ rotation of the workpiece in the 3-D infeed model.

At the first and third stages, a portion of the workpiece exists between the wheels. If η_{max} is the angular displacement difference between the point which has a maximum effective apparent depth of cut, $D_e(\theta, \eta_{max}, z_i)$, and an ideal contact point, $r(\theta, z_i)$ of layer i, the deflection of the system, $x(\theta, z_i)$, is

$$x(\theta, z_i) = \frac{f_o(\theta, z_i)}{(K_e/l_e)} \quad (13)$$
$$= \cos(\eta_{max})\{D_e(\theta, \eta_{max}, z_i) - L(\theta, \eta_{max}, z_i)\}$$

where $f_o(\theta, z_i)$ is the normal grinding force acting at layer i. If $r(\theta + \eta_k, z_i)$ is one of the grinding wheel contact points of this layer, the true depth of cut, $L(\theta, \eta_k, z_i)$, with its corresponding $D_e(\theta, \eta_k, z_i)$ is

$$L(\theta, \eta_k, z_i) = \frac{\cos(\eta_k) D_e(\theta, \eta_k, z_i) - x(\theta, z_i)}{\cos(\eta_k)} \quad (14)$$

$$(\text{when } \cos(\eta_k) D_e(\theta, \eta_k, z_i) \geq x(\theta, z_i))$$

When $\cos(\eta_k) D_e(\theta, \eta_k, z_i)$ is less than the deflection of the system, $x(\theta, z_i)$, the material removal will be zero. Thus, $f_o(\theta, z_i)$ can be formulated as a function of the true depth of cut as follows:

$$f_o(\theta, z_i) = \frac{K_m}{l_e} \left[\sum_{for \, all \, k} L(\theta, \eta_k, z_i) \right] + \frac{P_o}{l_e} \quad (15)$$

If there are positive $x(\theta, z_i)$ and $L(\theta, \eta_k, z_i)$, which satisfy Eqs. (13), (14), and (15) simultaneously, the actual material removal takes place. Therefore, if a peripheral point, $r_{old}(\theta + \eta_k, z_i)$, is ground at rotation θ, then this peripheral point just after grinding can be expressed as:

$$r_{new}(\theta + \eta_k, z_i) = r_{old}(\theta + \eta_k, z_i) - L(\theta, \eta_k, z_i) \quad (16)$$

The initial contact point between the workpiece and the grinding wheel is determined by finding the maximum displacement at the grinding wheel contact point in one revolution using the following equation:

$$\text{MAX} \left[-\frac{\sin\beta}{\sin(\alpha+\beta)} r(\phi-\alpha, 0) + \frac{\sin\alpha}{\sin(\alpha+\beta)} r(\phi-\pi+\beta, 0) + r(\phi-2\pi, 0) \right] \quad (17)$$
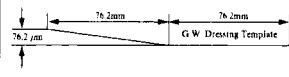
$$(0 \leq \phi < 2\pi)$$

where ϕ is a dummy parameter used to find the starting point.

5. Experiment and Simulation

The pre-grinding shape of the specimens in this experiment was a partially flat cylindrical hollow bar as shown in Fig. 4. This shape is easy to control and includes all orders of harmonics below the fortieth with the largest amplitudes obtained for the lowest orders (Rowe et al., 1965). It is useful to find any effect of the grinding variables on a certain order of waviness. Four

Table 1 Grinding conditions

Grinding Machine		Cincinnati OM-V
Center Height Angle (β)		6
Grinding Wheel	Specification	97A60K6VFM
	Outer Dia. (mm)	497.2
	Width (mm)	152.4
	Speed (rpm)	1240
Regulating Wheel	Specification	A80R2R
	Outer Dia. (mm)	288.0
	Width (mm)	203.2
	Speed (rpm)	20
	Tilt Angle	3
Work-rest Blade		Sintered Carbide
Blade Angle		60
Dressing Traverse Rate		40 μm/rev.
Through-feed G.W. Dressing Template		

Fig. 4 Details of the specimen geometry
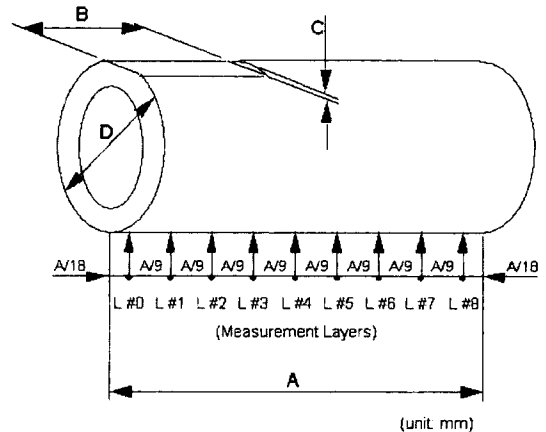
	Type	A ($\pm$0.3)	B	C ($\pm$0.004)	D ($\pm$0.002)
Through-feed	T0	74	0	0.05	23.534
	T1		74 $\pm$0.3		
	T2		49.3 $\pm$0.5		
	T3		24.7 $\pm$0.5		

types of cylindrical workpieces were used in this work. The first type of specimen had no flat. The second type of specimen had a flat along its axis. Also, the third and fourth types had flats whose lengths were 1/3 and 2/3 of the specimen length, respectively. The material of the specimens was
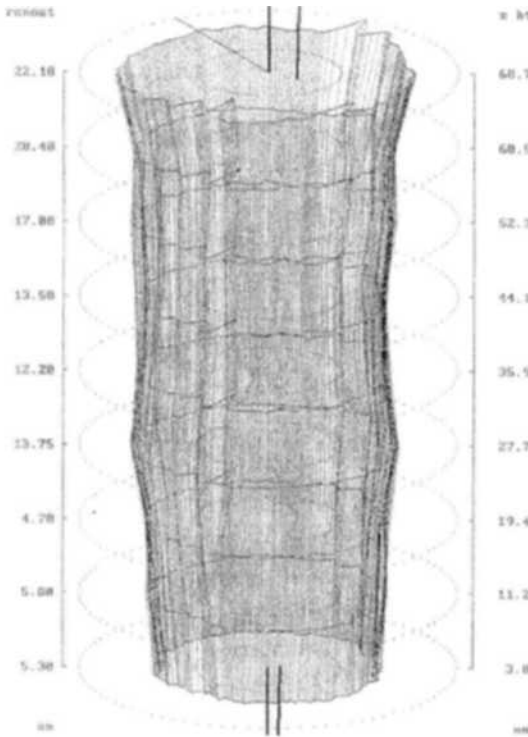
Fig. 5 Experimental result (specimen type: T2, leading end: flat end)
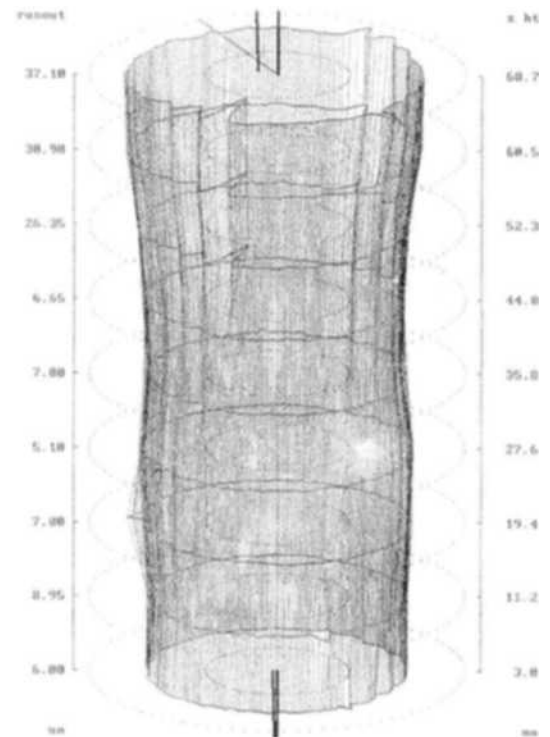
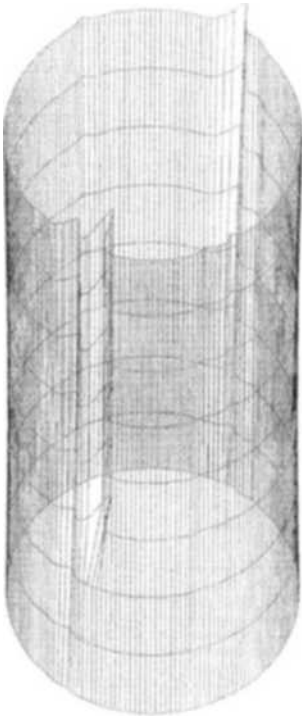**Fig. 6** Experimental result (specimen type: T3, leading end: flat end)

hardened steel with Rockwell C hardness of 62-63. The roundness error, straightness, and taper of the pre-grinding specimens, except the flat area, were within 2 μm, and the deviation of flat depth was within 4 μm. The grinding machine and conditions are given in Table 1.

To investigate the ground specimens 3-dimensionally, nine measuring layers (from 0 to 8) of each specimen were selected and their locations are shown in Fig. 4. The cylindricity profiles were measured on the Talyrond 252 machine from Rank Taylor Hobson Co. The measured cylindricity profiles are presented in Figs. 5 and 6.

To figure out the geometry of a ground workpiece, computer simulation techniques are applied to the analytical models. At the initial stage of through-feed grinding, only the leading end of the workpiece contacts the grinding wheel. At every incremental rotation, the new axial workpiece position is found, and whether a certain layer is between the wheels or not is identified. Also, the machining factor K_m, elasticity factor K_e, and threshold grinding force P_o are varied depending on the length of the engaged workpiece. To consider the effects of other workpieces, the effective apparent depth of cut, D_e, is used instead of D. To compute D_e, the grinding force of previous and/or following workpieces, F_c, is computed and given as an input data. When the correct L values are found, $r(\theta, z)$ as well as the reference contact lines and D must be renewed for the next step.

Each simulation was carried out under the corresponding experimental condition. The threshold grinding force, P_0 of 210 N was quoted from the reference (ASM International, 1989), and the machining factor, K_m, was calculated as 240 MN/m (Kim et al., 1992a, 1992b). The elasticity factor, K_e of 24 MN/m, was cited from the reference (Reshetov and Portman, 1988). Simulation results are shown in Figs. 7 and 8.

Fig. 7   Simulation result (specimen type : T2, leading end : flat end)
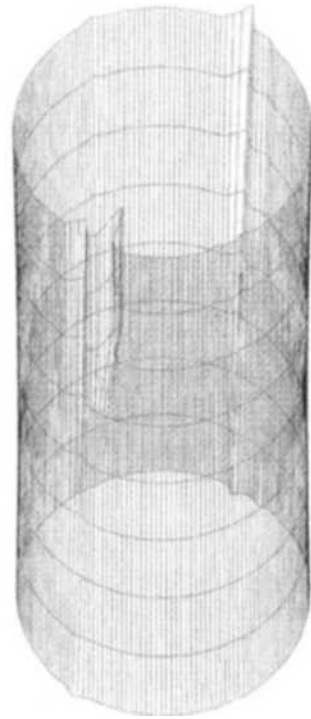
Fig. 8   Simulation result (specimen type : T3, leading end : flat end)

6. Results and Discussion

All the simulation results in Figs. 7 and 8 are similar to the corresponding experimental results given in Figs. 5 and 6. The number of lobes and the angular displacement of the peaks and the corresponding valleys are similar to what was shown in the infeed case (Kim et al., 1992b). Generally, as compared with the infeed case, all the results show smoother roundness profiles. From this, it can be found that a through-feed process is more stable than an infeed process. Also, simulation results show that the diameter varies along the axis. For type T3 specimens, the phase shift characteristic of peaks and valleys is also shown in both the simulated and experimentally obtained roundness profiles.

As compared with the infeed simulation, the through-feed simulation has a larger error range. Other than the experimental, measurement, and computational errors, the through-feed model has two important error factors in itself. One is the modeling of grinding force of the previous and/or following workpiece and the other is the assumption of global deflection of the grinding wheel.

$F_c(S)$ was introduced to incorporate the effect of other workpieces. To find this force, distribution of a grinding force along the grinding wheel axis, $f_{ss}(s)$, is required. Because only the current workpiece shape is known, geometry of other workpieces is assumed as a perfect cylinder. This perfectly cylindrical shape assumption is one of the reasons for the simulation error.

During a real grinding process, the grinding wheel deflects not only locally but also globally. The local deflection occurs at the workpiece contact region. The global deflection occurs in the machine system. In this model, the global deflection concept was added to the local deflection concept under the parallel deflection assumption to relate the effect of $F_c(S)$ on the apparent depth of cut of the current workpiece. As a result, the errors of two different deflections were

superposed.

7. Conclusion

A computer simulation method was developed to investigate the mechanism of cylindrical form generation in the centerless through-feed grinding process. To include the effects of other workpieces, a compensation force and global deflection were introduced.

For verification of this model, computer simulation results were compared with the experimental data. All the simulation results showed that the number of lobes and the angular displacement of peaks and valleys were similar to the corresponding experimental results. Also, these results showed that there is a phase shift characteristic of peaks and valleys.

Through this work, it was found that the ground shape is dependent not only on the grinding conditions and the physical properties of the workpiece but also on the pre-grinding shape (the type, size, and location of geometric errors) of the workpiece. Therefore, if there is a considerable variation in the pre-grinding workpiece shape, the geometric characteristics of the pre-grinding shape must be investigated and controlled.

References

ASM International, 1989, *Metals Handbook, 9th Edition, Vol. 16 Machining*, pp. 422, 448.

Dall, A. H., 1946, "Rounding Effect in Centerless Grinding," *Mechanical Engineering*, Vol. 68, No. 4, ASME, pp. 325~329.

Kim, K., Chu, C. N. and Barash, M. M., 1992a, "Roundness Generation during Centerless Infeed Grinding," *Transactions of NAMRI of SME*, 20, pp. 167~172.

Kim, K., Chu, C. N. and Barash, M. M., 1992b, *Cylindricity Control in Precision Centerless Grinding*, Technical Report TR-ERC 92-6, Purdue University, pp. 23~31, 77~86.

Meis, F. U., 1980, *Geometrische und kinematische Grundlagen fr das spitzenlose Durchlaufschleifen*, Ph. D. Dissertation, T. H. Aachen, W. Germany.

Reshetov, D. N. and Portman, V. T, 1988, *Accuracy of Machine Tools*, ASME Press, p. 275.

Rowe, W. B. and Barash, M. M., 1964, "Computer Method for Investigating the Inherent Accuracy of Centerless Grinding," *Int. J. Mach. Tool Des. Res.*, Vol. 4, pp. 91~116.

Rowe, W. B., Barash, M. M. and Koenigsberger, F., 1965, "Some Roundness Characteristics of Centerless Grinding," *Int. J. Mach. Tool Des. Res.*, Vol. 5, pp. 203~215.

Yonetsu, S., 1959, "Forming Mechanism of Cylindrical Work in Centerless Grinding," *Proc. Fujihara Memorial Faculty of Engineering*, Keio Univ., Vol. 12, No. 47, pp. 27~45.

Yonetsu, S., 1960, "Consideration on the Control Wheel Truing of a Centerless Grinder," *Proc. Fujihara Memorial Faculty of Engineering*, Keio Univ., Vol. 13, No. 49, pp. 1~9.